Bioactive Materials 14 (2022) 145–151

Contents lists available at ScienceDirect

Bioactive Materials

journal homepage: www.keaipublishing.com/en/journals/bioactive-materials

Magnetic covalent organic framework nanospheres-based miRNA biosensor for sensitive glioma detection

Dong Liang [a,1], Xiaoyi Zhang [a,1], Yi Wang [b,**], Taotao Huo [a], Min Qian [a], Yibo Xie [a], Wenshuai Li [a], Yunqiu Yu [a,***], Wei Shi [c], Qianqian Liu [c], Junle Zhu [d], Chun Luo [d], Zhijuan Cao [a], Rongqin Huang [a,*]

[a] School of Pharmacy, Key Laboratory of Smart Drug Delivery, Ministry of Education, Fudan University, Shanghai, 201203, China
[b] Center for Advanced Low-dimension Materials, State Key Laboratory for Modification of Chemical Fibers and Polymer Materials, College of Chemistry, Chemical Engineering and Biotechnology, Donghua University, Shanghai, 201600, China
[c] Department of Neurosurgery, Affiliated Hospital of Nantong University, Nantong, 226001, China
[d] Department of Neurosurgery, Tongji Hospital, Tongji University School of Medicine, Shanghai, 200065, China

ARTICLE INFO

Keywords:
Blood samples
Fluorescence signal amplification biosensor
Glioma diagnosis
Magnetic COF nanospheres
miRNA detection

ABSTRACT

Sensitive detection and accurate diagnosis/prognosis of glioma remain urgent challenges. Herein, dispersed magnetic covalent organic framework nanospheres (MCOF) with uniformed Fe_3O_4 nano-assembly as cores and high-crystalline COF as shells were prepared by monomer-mediated in-situ interface growth strategy. Based on the unique interaction between MCOF and hairpin DNA, a fluorescent signal amplified miRNA biosensor was constructed. It could realize the sensitive detection of miRNA-182 in different matrixes, where the detection limit, linearity range and determination coefficient (R^2) in real blood samples reached 20 fM, 0.1 pM–10 pM and 0.991, respectively. Also, it possessed good stability and precision as observed from the low intra-day/inter-day RSD and high extraction recovery. As a result, it could quantify miRNA-182 in serum of glioma patients, the concentration of which was significantly higher than that of healthy people and obviously decreased after surgery. Finally, a proof-of-concept capillary chip system using this biosensor was proposed to realize the visualized detection of miRNA-182 in microsample. These findings suggest a robust way for sensitive detection and accurate diagnosis/prognosis of glioma.

1. Introduction

The low survival rates of glioma patients have spurred researchers to develop various strategies for glioma treatment [1,2]. Clinically, surgery, combined radiotherapy or chemotherapy remains the main treatment for glioma [3]. Unfortunately, glioma is difficult to be discovered owing to its special location in central nervous system (CNS), which would result in missing the optimal treatment period for most glioma patients after diagnosed [4]. Therefore, timely early detection and accurate diagnosis of glioma are ultimately important for the effective clinical treatments. Currently, imaging methods such as magnetic resonance imaging (MRI) and computed tomography (CT) are often adopted to detect tumor occurrence [5]. However, they are incapable of differentiating the benign and malignant lesions especially with early small sizes. Although the tissue biopsy could improve the accuracy, its invasion is not beneficial for the diagnosis of glioma in CNS. Comparatively, liquid biopsy based on tumor markers in biological fluids (including miRNAs, ctDNAs, proteins, exosomes and CTCs) shows great promise for cancer diagnosis due to its simplicity, rapidity and non-invasion [6–11]. Among these, miRNAs, as small non-coding RNAs that target corresponding messenger RNAs to post-transcriptionally down-regulate certain gene expression, exhibit high specificity during the tumorigenesis, which therefore could be utilized for the tumor liquid biopsy [12,13]. Recently, miRNA-182, being found to play an important

Peer review under responsibility of KeAi Communications Co., Ltd.
* Corresponding author.
** Corresponding author.
*** Corresponding author.
E-mail address: rqhuang@fudan.edu.cn (R. Huang).
[1] These authors contribute equally to this work.

https://doi.org/10.1016/j.bioactmat.2021.11.033
Received 16 August 2021; Received in revised form 26 October 2021; Accepted 21 November 2021
Available online 18 December 2021

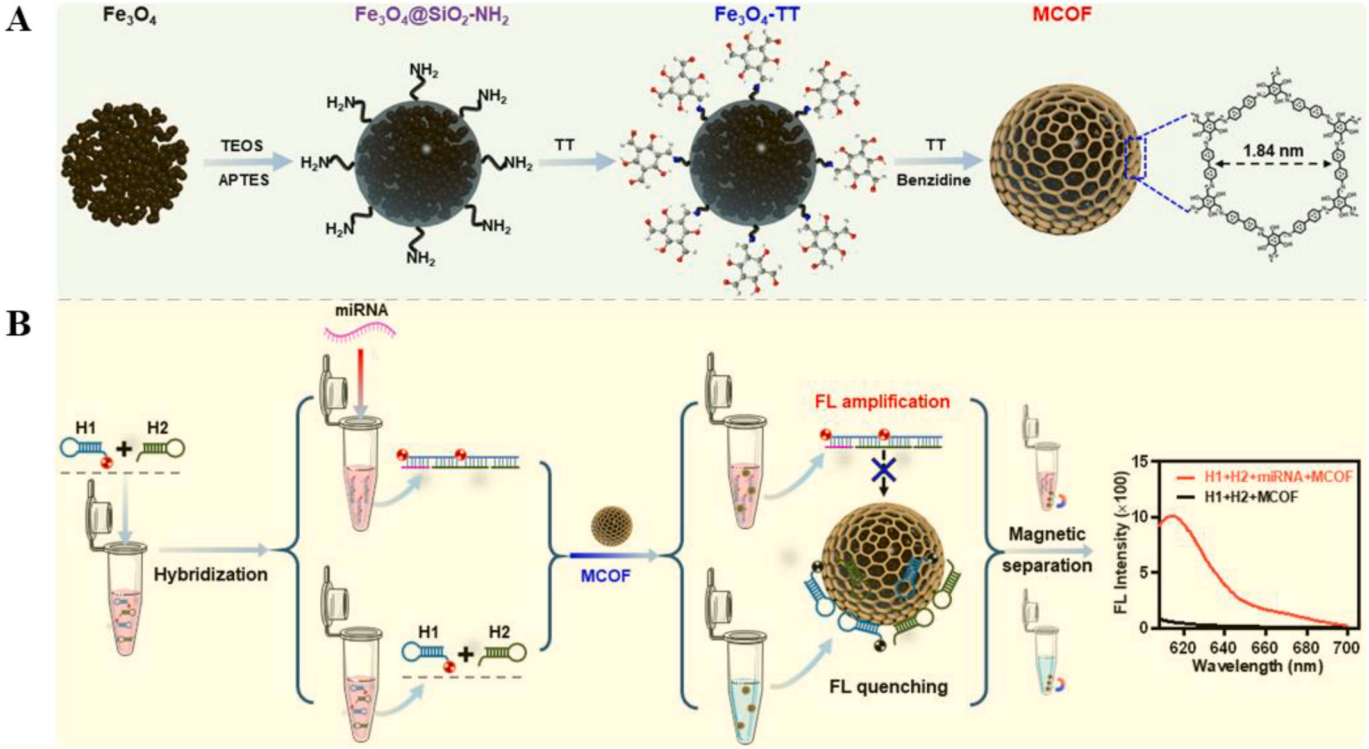

Scheme 1. Schematic diagram of synthesis and detection. (A) The dispersed and high-crystalline COF-coated Fe_3O_4 magnetic nanospheres (MCOF) prepared by monomer-mediated in-situ interface growth strategy. (B) The fluorescent signal amplified miRNA biosensor constructed by using two hairpin DNA probes.

regulatory role in the proliferation and invasion of glioma cells [14], has been reported to indicate the occurrence and development of glioma with high specificity [15], and thus can serve as the special marker for the accurate glioma diagnosis or even the prognosis monitoring [16]. However, the scarce miRNA-182 spiked in the human blood with complex components makes it a great challenge to achieve the sensitive

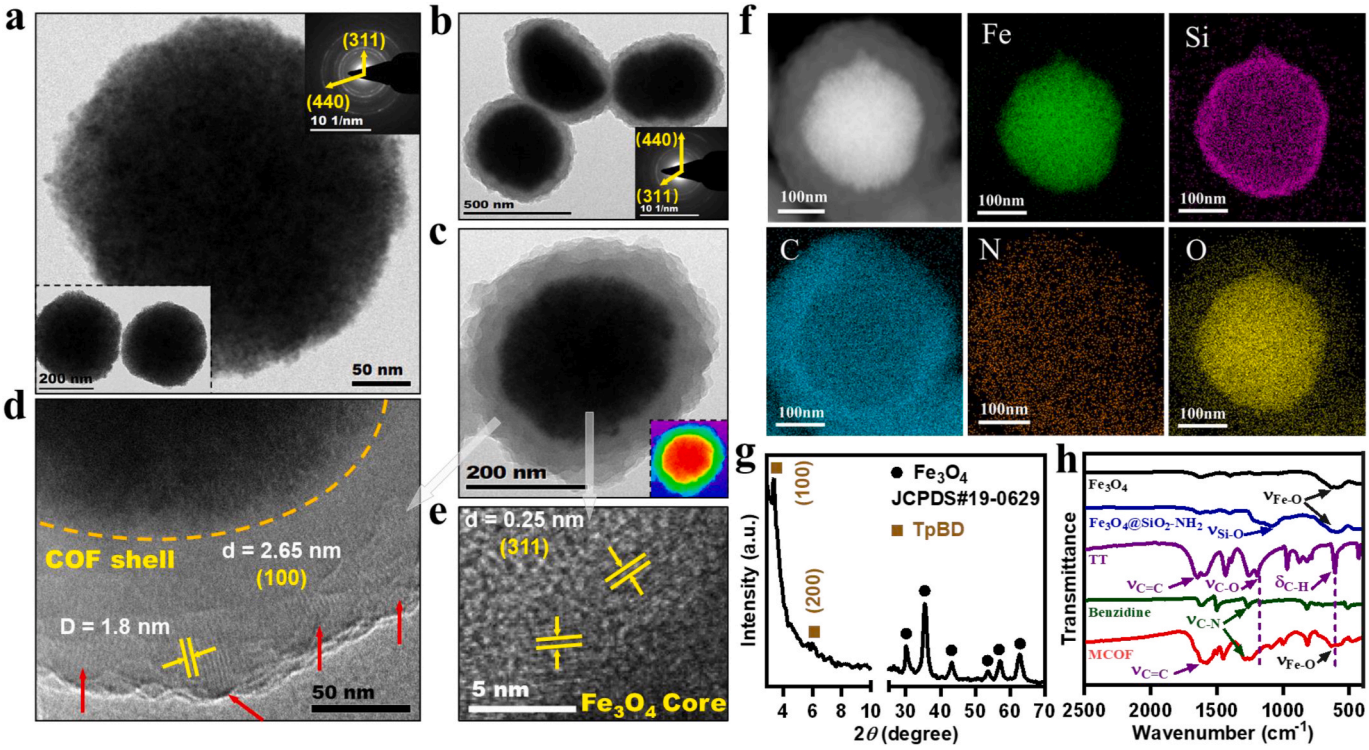

Fig. 1. Characterizations of MCOF. (a) TEM images and ED pattern (inset) of magnetic Fe_3O_4 nano-assembly. (b) TEM image and ED pattern of multiple MCOF nanospheres. (c) TEM image of single MCOF nanosphere. (d) HRTEM image of COF shell. (e) HRTEM image of magnetic Fe_3O_4 core. (f) STEM image and EDS element mappings of MCOF. (g) XRD pattern of MCOF. (h) FT-IR spectra for monomers (TT, Benzidine), mid products (Fe_3O_4, Fe_3O_4@SiO_2) and MCOF nanospheres.

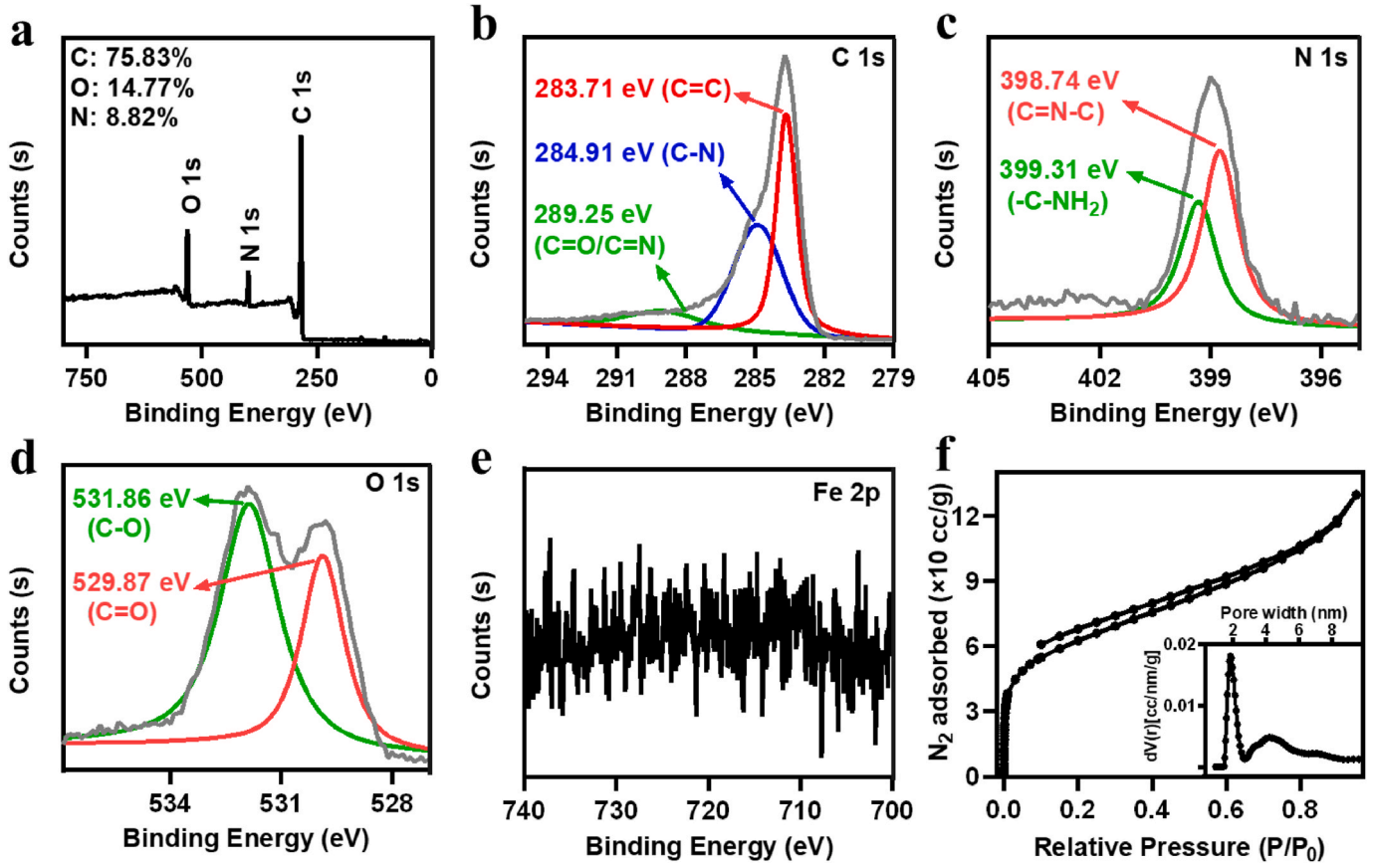

Fig. 2. Structural analysis of MCOF. (a) XPS survey spectrum and corresponding (b) C 1s, (c) N 1s, (d) O 1s and (e) Fe 2p spectra. (f) Nitrogen adsorption-desorption isotherms and pore size distribution curve.

detection [17].

As a simple and effective isothermal signal amplification technique, hybrid chain reaction has recently been used for biosensing, bioimaging and biomedicine, and also shows superiority in low-content miRNA detection [18]. Nevertheless, the hybridization chain reaction requires a suitable signal amplification sensing platform. Although traditional fluorescence quenchers such as graphene, molybdenum disulfide, black phosphorus (BP) nanosheets, polymeric nanoparticles exhibit potentials for the fluorescence "turn-on" sensing detection of nucleic acid through π-π interaction and distinctive superiorities in biomedical applications [19–23], traditional 2D materials are not beneficial for the sensitive biosensing due to the weak interactions between the materials and the hairpin DNA. The platforms to synergize this "turn-on" sensing with fluorescence signal amplification based on hairpin DNA hybridization for enhanced miRNA detection are seldom exploited. Most recently, two-dimensional COF nanosheets have been found with the capability of combing hybrid chain reaction to achieve fluorescence signal amplification-based DNA sensing via the sensitive interactions between the crystalline COF framework and the special hairpin DNA strands [24]. However, most COF nanosheets suffer from severely aggregation, low crystallization and easy degradation (instability) [25], which greatly depresses their biosensing performances. Moreover, the two-dimensional nanosheets with sharp edges cannot fulfill their interactions with the DNA molecules [26]. And also, the pristine COF organic nanomaterials are sneaked into complicated detection system (blood), thus troubling the isolation during the detection. All these would worsen the sensitivity and stability of COF-based fluorescence biosensors. Therefore, preparation of spherical COF nanoparticles with high crystallinity to fulfill their interactions with the DNA molecules and simultaneously endow them with convenient magnetic separation properties are urgently demanded for sensitive miRNA detection and fast glioma diagnosis/prognosis [27].

In this work, the dispersed and high-crystalline COF-coated Fe_3O_4 magnetic nanospheres (MCOF) were prepared by monomer-mediated in-situ interface growth strategy (Scheme 1A). Consequently, a fluorescent signal amplified miRNA biosensor was constructed by using two hairpin DNA probes (Scheme 1B). Taking virtues of the special magnetic COF nanospheres and the unique sensing system, this miRNA biosensor could realize the sensitive detection of miRNA-182 in different matrixes. Moreover, this biosensor could quantify the miRNA-182 in serum of glioma patients, which displayed low detection limits, wide linearity range and high stability. It was found that miRNA-182 in the serum of glioma patients was significantly higher than that of healthy people and obviously decreased after surgery. Finally, a visualization strategy for sensitive miRNA-182 detection in micro-sample was also proposed by using this biosensor with a capillary system. All these paved a robust way for convenient detection and accurate diagnosis/prognosis of glioma.

2. Results and discussion

To construct the MCOF-based fluorescence signal amplification biosensor, magnetic Fe_3O_4 nanospheres (~310 nm) assembled by ultrasmall crystalline nanoparticles (Fig. 1a) were firstly prepared via the solvothermal synthesis. Then, aminated silica were uniformly coated on the Fe_3O_4 nanospheres via the interface hydrolysis-condensation reaction of silane to facilitate the 2,4,6-Trihydroxybenzene-1,3,5-tricarbaldehyde (TT) monomer linkage, whereafter the crystalline COF could be grown on the surfaces of the nanospheres by the monomer-mediated in-situ polymerization (Scheme 1A). The as-synthesized nanoparticles were dispersed nanospheres (~430 nm) with distinct core-shell structure (Fig. 1b and c, Table S1). The cores kept crystalline Fe_3O_4 indexed

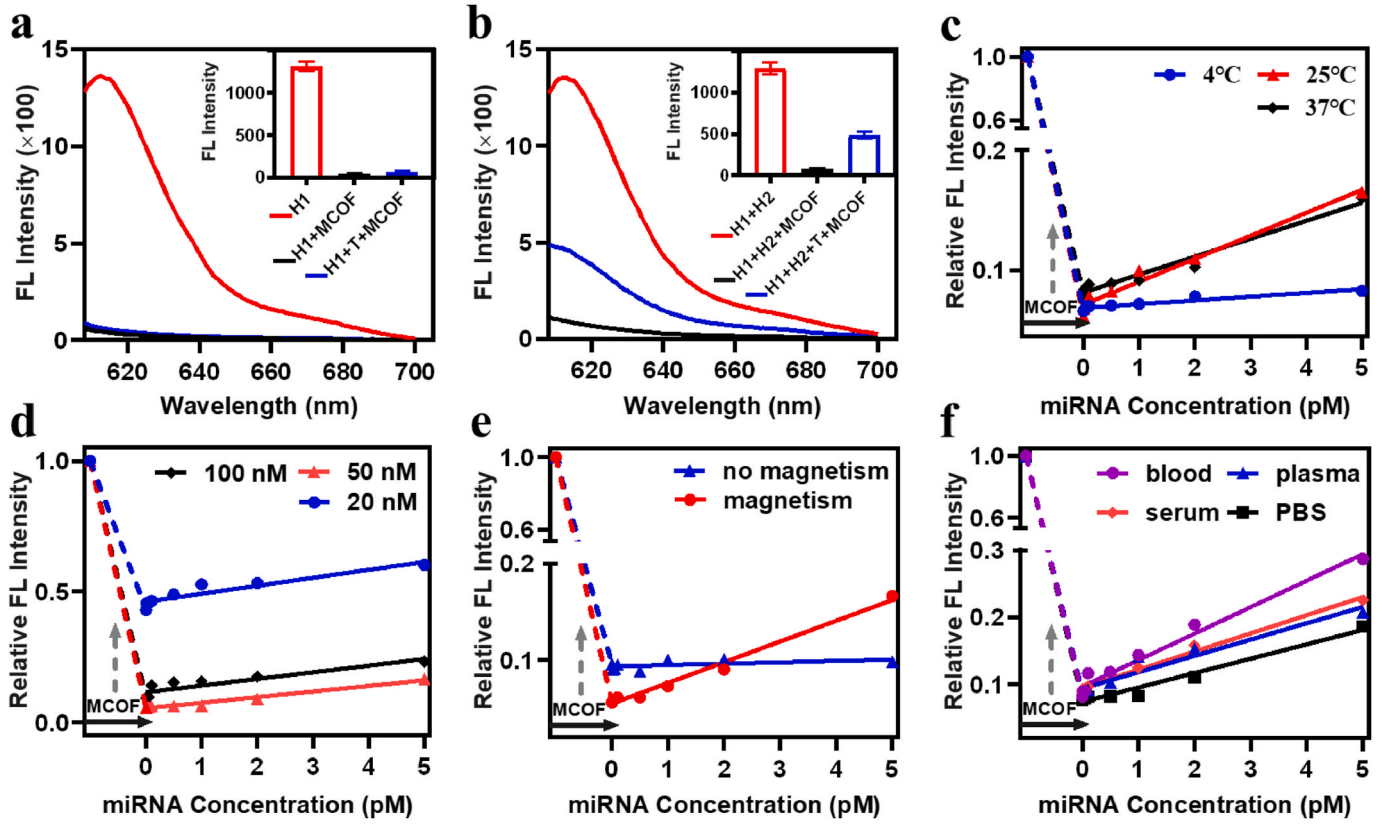

Fig. 3. Optimizations of the fluorescence signal amplification biosensor. (a, b) Fluorescence spectra of the fluorescence signal amplification biosensor for the miRNA biosensing in the absence of H2 and in the simultaneous presence of H1 and H2, respectively. (c–f) Relative fluorescence intensities of the fluorescence signal amplification biosensor for the miRNA biosensing at different hybrid chain reaction temperatures, at different H1 and H2 probe concentrations, with or without magnetic separation, and in different media, respectively.

by its obvious lattice fringes of (311) planes and typical ED patterns of (311)/(440) planes, while the shells were about 60 nm in thickness and possessed obviously ordered micropores with a pore size of about 1.8 nm. Interestingly, these microporous channels in the shell were almost vertical to the core surfaces (Fig. 1d and e). These revealed the high orderliness of the shell, which would be the crystalline COF layer. Further characterizations by STEM image and EDS element mappings confirmed the core-shell architecture with the Fe/O species as core and the dominated C/N species as shell. Notably, a silica layer sandwiched between the Fe/O core and the C/N shell was clearly observed (Fig. 1f and Fig. S1), verifying the aminated silica-grafted TT monomer for in-situ interface growth of COF. Meanwhile, XRD pattern also revealed the magnetic COF nanoparticles as it simultaneously exhibited characteristic COF peaks at low angles of 3.3° (100) and 6.0° (200) [28], and typical magnetic Fe_3O_4 peaks at high angles (Fig. 1g). Additionally, FT-IR also suggested the aminated silica coating on Fe_3O_4 followed by TT-grafting and then COF growth, as indicated by the successively added Si–O stretching vibration (1100 cm^{-1}) from aminated silica, C═C stretching vibration (1600 cm^{-1}) from TT and C–N stretching vibration (1295 cm^{-1}) from benzidine as well as the decreased C–O stretching vibration (1192 cm^{-1}) and C–H bending vibration (606 cm^{-1}) from the polymerizations between the –CHO group and $–NH_2$ group, respectively (Fig. 1h).

Further investigations into MCOF by XPS confirmed C, O, and N elements, and the atomic ratios were calculated to be 75.83%, 14.77% and 8.82% on the surfaces, respectively (Fig. 2a). The dominated C═C bond at 283.71 eV and C═N–C bond at 398.74 eV in deconvoluted C1s and N1s [29], respectively, revealed the crystalline COF framework via the polymerizations between TT and Benzidine (Fig. 2b and c). Meanwhile, the minor C═O bond and -C-NH_2 bond as well as the obvious oxygen-contained bonds in deconvoluted C1s, N1s and O1s [30], respectively, suggested some unreacted groups terminated on the surfaces, which promised the water dispersity of MCOF (Fig. 2c and d). Moreover, no obvious Fe signals in XPS confirmed the well-coated Fe_3O_4 cores by COF shells, which could not be detected by the surface elements analysis (XPS) (Fig. 2e). In these MCOF nanoparticles, the COF layer had about 54 wt% content and good thermal stability (>300 °C) (Fig. S2). As a result, the BET surface area and pore volume of MCOF reached 224 m^2/g and 0.32 cc/g, respectively, as measured by the N_2 adsorption-desorption isotherms (Fig. 2f). Also, uniformed micropores of 1.84 nm, in good agreement with the measurements by HRTEM, emerged in pore size distribution cures, validating the highly crystalline COF coating. All these suggested well-prepared magnetic COF nanospheres of MCOF, which could be easily dispersed in the water, ethanol and PBS, and achieve fast separation under the magnetic field for further applications (Fig. S3).

Owing to the well-architected structure and unique properties, MCOF could be exploited as the fluorescence signal amplification biosensor through its differentiated adsorption (hydrogen bonding and π-π interaction)-mediated fluorescence (FL) quenching or amplification for the double-stranded DNA (dsDNA) and the hairpin DNA, respectively (Scheme 1B). Therefore, selecting a special hairpin DNA probe 2 (H2) and a suitable fluorescence Texas Red-labeled hairpin DNA probe 1 (H1) to hybridize the targeted miRNA (Table S2) into dsDNA, this MCOF-based biosensor could realize the sensitive detection of miRNA-182, an important biomarker in the blood to indicate the oncogenesis and development of glioma [16]. As shown in Fig. 3a, MCOF quenched the fluorescence of H1 via the special adsorption. However, this quenching reserved after adding targeted miRNA-182 (T) because of the incapability of forming dsDNA under the absence of H2. Comparatively, in the simultaneous presence of H1 and H2, MCOF still quenched the fluorescence of H1, but this quenching was significantly blocked under the

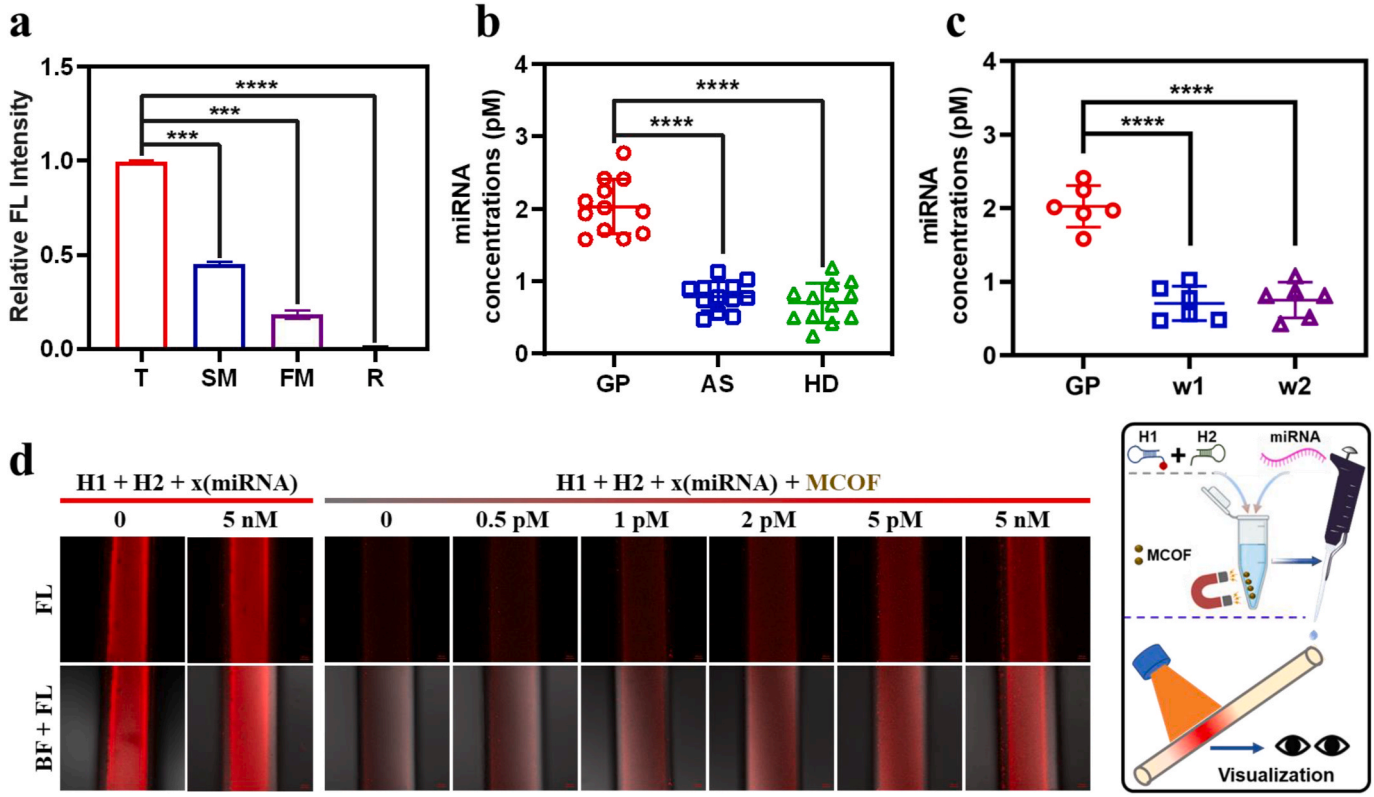

Fig. 4. The miRNA-182 detection using the MCOF-based biosensor and a capillary-assisted visualization system. (a) Relative fluorescence intensities of the MCOF-based biosensor upon exposure to different miRNA molecules. (T: Target miRNA; SM: Single-base mismatch miRNA; FM: Four-base mismatch miRNA; R: Random miRNA. (b) Concentrations of miRNA-182 from blood samples of 12 healthy donors, 12 glioma patients before and after surgery determined by the MCOF-based biosensor. (GP: glioma patients before surgery; AS: after surgery; HD: healthy donors). (c) Concentrations of miRNA-182 from blood samples of 6 glioma patients before and after surgery determined by the MCOF-based biosensor. (GP: glioma patients before surgery; w1: one week after surgery; w2: two weeks after surgery). (d) Fluorescence images and schematic illustration of the capillary-assisted MCOF-based visualized sensing systems upon exposure to different concentrations of miRNA-182 molecules. Data are expressed as Mean ± SD. ***: $p < 0.001$; ****: $p < 0.0001$.

Table 1
Intra-day and inter-day precision, extraction recovery of miRNA-182 assay using the MCOF-based biosensor (mean ± SD, n = 5).

Concentration (pM)	Inter-day RSD (%)	Intra-day RSD (%)	Extraction Recovery (%)
5.0	3.37	1.00	92.42 ± 5.04
2.0	4.49	2.93	96.72 ± 4.01
1.0	6.31	3.57	98.97 ± 7.15
0.1	6.56	2.38	94.23 ± 6.46

Table 2
Concentrations of miRNA-182 from blood samples of 12 healthy donors, 12 glioma patients before and after surgery determined by the MCOF-based biosensor.

	Patients before surgery (pM)	Patients after surgery (pM)	Healthy donors (pM)
	1.656 ± 0.034	0.733 ± 0.080	0.961 ± 0.074
	2.415 ± 0.027	0.921 ± 0.023	0.508 ± 0.085
	2.105 ± 0.018	0.892 ± 0.021	1.002 ± 0.029
	1.575 ± 0.029	0.749 ± 0.019	0.246 ± 0.038
	2.767 ± 0.050	1.127 ± 0.060	0.862 ± 0.069
	1.704 ± 0.074	0.509 ± 0.030	0.520 ± 0.084
	1.961 ± 0.047	0.773 ± 0.058	0.499 ± 0.063
	1.582 ± 0.089	0.562 ± 0.064	0.423 ± 0.094
	2.242 ± 0.035	0.911 ± 0.048	0.810 ± 0.082
	1.933 ± 0.075	0.474 ± 0.009	0.781 ± 0.088
	2.409 ± 0.074	0.776 ± 0.045	0.683 ± 0.084
	2.014 ± 0.015	1.024 ± 0.087	1.186 ± 0.054
Average	2.036 ± 0.394	0.791 ± 0.211	0.681 ± 0.274

existence of miRNA-182 due to its hybridization with H1 and H2 into non-adsorbable dsDNA (Fig. 3b). In this event, miRNA-182 could be quantified by comparing the fluorescence intensities before and after its addition. Much importantly, one miRNA-182 molecule could initiate the multiple hybridization with numerous H1 and H1 into dsDNA, which therefore was the fluorescence amplification process mediated by the MCOF-based biosensor. Benefiting from this behavior, the biosensor also exhibited miRNA concentration responsive relative fluorescence intensity under different conditions, where the detection temperature at 25 °C, H1+H2 probe concentration of 50 nM and synergism with magnetism separation contributed the optimal linear relationship with maximal R^2 (Fig. 3c–e, Fig. S4, and Tables S3–5). Correspondingly, this biosensor could detect miRNA with good linearity in different media including phosphate buffered saline (PBS), serum, plasma and even blood (Fig. 3f, and Table S6). In the real human serum, the detection limit, linearity range and determination coefficient (R^2) reached 20 fM, 0.1 pM–10 pM, and 0.991, respectively (Fig. S5), which were much more superior to those fluorescent miRNA detections in previous reports (Table S7). Moreover, this biosensor had high specificity to the target miRNA, where even the single-base mismatch sequences (SM) did not cause significant interferences to the relative fluorescence intensity (Fig. 4a). In addition, this biosensor possessed good stability and precision, where the intra-day/inter-day RSD and extraction recovery reached 6.56%/2.38% and 94.23 ± 6.46%, respectively, even at a very low miRNA concentration of 0.1 pM (Table 1).

Since the MCOF-based biosensor could selectively detect low concentration of glioma miRNA-182 in the blood, it was expected that this biosensor could serve for the glioma diagnosis and prognosis. To

validate this, human blood samples from glioma patients before and after surgery were collected and subjected to miRNA-182 detection using the MCOF-based biosensor. As shown in Fig. 4b and Table 2, the average concentrations of miRNA-182 in the blood of glioma patients before surgery were all significantly higher than those for healthy people. One week after surgery, the values were obviously decreased to approximate the normal level (Fig. 4c) and then maintained in this level to 2 weeks, which indicated the potential of the biosensor to detect postoperative recovery. These suggested the MCOF-based biosensor could be used for practical glioma diagnosis and prognosis via its sensitive quantification of the glioma biomarker (miRNA-182) in blood.

In practical applications, it would be prevailed to take blood as little as possible for the detection. Therefore, a capillary-assisted visualization system was exploited as the proof of concept for micro sample detection using the MCOF-based biosensor. As shown in Fig. 4d, only H1 + H2 could not probe the miRNA due to the unchanged fluorescence in capillary after miRNA addition. However, the red fluorescence in capillary was gradually enhanced with the increased miRNA addition when using the MCOF as the sensing platform. This special and sensitive biosensing performances were in good agreement with the above measurements by fluorescence spectra. Herein, the micro samples were used and the outcomes could be directly visualized, which would be great promising for the practical diagnosis application.

3. Conclusion

In this work, a monomer-mediated in-situ growth strategy was exploited for the preparation of dispersed magnetic COF nanospheres (MCOF). This MCOF possessed uniformed magnetic Fe_3O_4 nanoparticles as core and high-crystalline COF as shell, which thus exhibited obvious water-dispersity with fast magnetic separation and highly ordered micropores with their channels almost vertical to the core surfaces. Consequently, a fluorescence signal amplified miRNA biosensor was constructed by using MCOF and two hairpin DNA probes. Attributing to the special fluorescence quenching or amplification induced by the different adsorption of double-stranded DNA (dsDNA) or hairpin DNA on MCOF, this MCOF-based biosensor could realize the sensitive quantification of miRNA-182 in even the real patient blood. As a result, it was found that the obviously high concentration of miRNA-182 for glioma patients was significantly decreased after surgery. Moreover, this biosensor could also achieve the visualized detection of miRNA-182 in micro-sample via the proof-of-concept capillary chip system. All these findings showed great potential of this MCOF-based biosensor for accurate diagnosis and prognosis of glioma.

CRediT authorship contribution statement

Dong Liang: Methodology, Validation, Formal analysis, Investigation, Writing – original draft, Visualization. **Xiaoyi Zhang:** Validation, Methodology, Investigation. **Yi Wang:** Conceptualization, Methodology, Writing – review & editing, Project administration. **Taotao Huo:** Methodology. **Min Qian:** Methodology. **Yibo Xie:** Visualization. **Wenshuai Li:** Formal analysis. **Yunqiu Yu:** Conceptualization, Methodology, Supervision. **Wei Shi:** Resources. **Qianqian Liu:** Resources. **Junle Zhu:** Resources. **Chun Luo:** Resources. **Zhijuan Cao:** Conceptualization. **Rongqin Huang:** Conceptualization, Methodology, Writing – review & editing, Project administration.

Declaration of competing interest

The authors declare no conflicts of interest.

Acknowledgements

This work was supported by National Natural Science Foundation of China (31922044, 81861138040, 81773280, 82172746 and 81974453), Program of Shanghai Academic Research Leader (20XD1420500), Natural Science Foundation of Shanghai (19ZR1471600), and Jiangsu Provincial Science and Technology Department Social Development–Clinical Frontier Technology (BE2020769).

Appendix A. Supplementary data

Supplementary data to this article can be found online at https://doi.org/10.1016/j.bioactmat.2021.11.033.

References

[1] Q.T. Ostrom, N. Patil, G. Cioffi, K. Waite, C. Kruchko, J.S. Barnholtz-Sloan, CBTRUS statistical report: primary brain and other central nervous system tumors diagnosed in the United States in 2013-2017, Neuro Oncol. 22 (2020) iv1–iv96.
[2] M.R. Gilbert, J.J. Dignam, T.S. Armstrong, J.S. Wefel, D.T. Blumenthal, M. A. Vogelbaum, H. Colman, A. Chakravarti, S. Pugh, M. Won, R. Jeraj, P.D. Brown, K.A. Jaeckle, D. Schiff, V.W. Stieber, D.G. Brachman, M. Werner-Wasik, I. W. Tremont-Lukats, E.P. Sulman, K.D. Aldape, W.J. Curran Jr., M.P. Mehta, A randomized trial of bevacizumab for newly diagnosed glioblastoma, N. Engl. J. Med. 370 (2014) 699–708.
[3] N. Sanai, M.S. Berger, Surgical oncology for gliomas: the state of the art, Nat. Rev. Clin. Oncol. 15 (2018) 112–125.
[4] J. Fangusaro, A. Onar-Thomas, T. Young Poussaint, S. Wu, A.H. Ligon, N. Lindeman, A. Banerjee, R.J. Packer, L.B. Kilburn, S. Goldman, I.F. Pollack, I. Qaddoumi, R.I. Jakacki, P.G. Fisher, G. Dhall, P. Baxter, S.G. Kreissman, C. F. Stewart, D.T.W. Jones, S.M. Pfister, G. Vezina, J.S. Stern, A. Panigrahy, Z. Patay, B. Tamrazi, J.Y. Jones, S.S. Haque, D.S. Enterline, S. Cha, M.J. Fisher, L.A. Doyle, M. Smith, I.J. Dunkel, M. Fouladi, Selumetinib in paediatric patients with BRAF-aberrant or neurofibromatosis type 1-associated recurrent, refractory, or progressive low-grade glioma: a multicentre, phase 2 trial, Lancet Oncol. 20 (2019) 1011–1022.
[5] M.J. van den Bent, Interobserver variation of the histopathological diagnosis in clinical trials on glioma: a clinician's perspective, Acta Neuropathol. 120 (2010) 297–304.
[6] Y.Y. Broza, X. Zhou, M. Yuan, D. Qu, Y. Zheng, R. Vishinkin, M. Khatib, W. Wu, H. Haick, Disease detection with molecular biomarkers: from chemistry of body fluids to nature-inspired chemical sensors, Chem. Rev. 119 (2019) 11761–11817.
[7] A.M. Lennon, A.H. Buchanan, I. Kinde, A. Warren, A. Honushefsky, A.T. Cohain, D. H. Ledbetter, F. Sanfilippo, K. Sheridan, D. Rosica, C.S. Adonizio, H.J. Hwang, K. Lahouel, J.D. Cohen, C. Douville, A.A. Patel, L.N. Hagmann, D.D. Rolston, N. Malani, S. Zhou, C. Bettegowda, D.L. Diehl, B. Urban, C.D. Still, L. Kann, J. I. Woods, Z.M. Salvati, J. Vadakara, R. Leeming, P. Bhattacharya, C. Walter, A. Parker, C. Lengauer, A. Klein, C. Tomasetti, E.K. Fishman, R.H. Hruban, K. W. Kinzler, B. Vogelstein, N. Papadopoulos, Feasibility of blood testing combined with PET-CT to screen for cancer and guide intervention, Science (2020) 369.
[8] D.N. Louis, A. Perry, G. Reifenberger, A. von Deimling, D. Figarella-Branger, W. K. Cavenee, H. Ohgaki, O.D. Wiestler, P. Kleihues, D.W. Ellison, The 2016 World Health Organization classification of tumors of the central nervous system: a summary, Acta Neuropathol. 131 (2016) 803–820.
[9] J. Buckner, C. Giannini, J. Eckel-Passow, D. Lachance, I. Parney, N. Laack, R. Jenkins, Management of diffuse low-grade gliomas in adults - use of molecular diagnostics, Nat. Rev. Neurol. 13 (2017) 340–351.
[10] G. Reifenberger, H.G. Wirsching, C.B. Knobbe-Thomsen, M. Weller, Advances in the molecular genetics of gliomas - implications for classification and therapy, Nat. Rev. Clin. Oncol. 14 (2017) 434–452.
[11] G. Siravegna, S. Marsoni, S. Siena, A. Bardelli, Integrating liquid biopsies into the management of cancer, Nat. Rev. Clin. Oncol. 14 (2017) 531–548.
[12] R. Rupaimoole, F.J. Slack, MicroRNA therapeutics: towards a new era for the management of cancer and other diseases, Nat. Rev. Drug Discov. 16 (2017) 203–222.
[13] L. Wu, X. Qu, Cancer biomarker detection: recent achievements and challenges, Chem. Soc. Rev. 44 (2015) 2963–2997.
[14] L. Song, L. Liu, Z. Wu, Y. Li, Z. Ying, C. Lin, J. Wu, B. Hu, S.Y. Cheng, M. Li, J. Li, TGF-beta induces miR-182 to sustain NF-kappaB activation in glioma subsets, J. Clin. Invest. 122 (2012) 3563–3578.
[15] S.D. Weeraratne, V. Amani, N. Teider, J. Pierre-Francois, D. Winter, M.J. Kye, S. Sengupta, T. Archer, M. Remke, A.H. Bai, P. Warren, S.M. Pfister, J.A. Steen, S. L. Pomeroy, Y.J. Cho, Pleiotropic effects of miR-183~96~182 converge to regulate cell survival, proliferation and migration in medulloblastoma, Acta Neuropathol. 123 (2012) 539–552.
[16] L. Jiang, P. Mao, L. Song, J. Wu, J. Huang, C. Lin, J. Yuan, L. Qu, S.Y. Cheng, J. Li, miR-182 as a prognostic marker for glioma progression and patient survival, Am. J. Pathol. 177 (2010) 29–38.
[17] M.K. Masud, M. Umer, M.S.A. Hossain, Y. Yamauchi, N.T. Nguyen, M.J. A. Shiddiky, Nanoarchitecture frameworks for electrochemical miRNA detection, Trends Biochem. Sci. 44 (2019) 433–452.
[18] S. Bi, S. Yue, S. Zhang, Hybridization chain reaction: a versatile molecular tool for biosensing, bioimaging, and biomedicine, Chem. Soc. Rev. 46 (2017) 4281–4298.
[19] Y.X. Lin, Y. Wang, J. Ding, A. Jiang, J. Wang, M. Yu, S. Blake, S. Liu, C.J. Bieberich, O.C. Farokhzad, L. Mei, H. Wang, J. Shi, Reactivation of the tumor suppressor

PTEN by mRNA nanoparticles enhances antitumor immunity in preclinical models, Sci. Transl. Med. 13 (2021).
[20] F. Zhang, G. Lu, X. Wen, F. Li, X. Ji, Q. Li, M. Wu, Q. Cheng, Y. Yu, J. Tang, L. Mei, Magnetic nanoparticles coated with polyphenols for spatio-temporally controlled cancer photothermal/immunotherapy, J. Contr. Release 326 (2020) 131–139.
[21] W. Tao, X.B. Zhu, X.H. Yu, X.W. Zeng, Q.L. Xiao, X.D. Zhang, X.Y. Ji, X.S. Wang, J. J. Shi, H. Zhang, L. Mei, Black phosphorus nanosheets as a robust delivery platform for cancer theranostics, Adv. Mater. 29 (2017).
[22] Z. Shi, Y. Zhou, T. Fan, Y. Lin, H. Zhang, L. Mei, Inorganic nano-carriers based smart drug delivery systems for tumor therapy, Smart Mater. Med. 1 (2020) 32–47.
[23] C. Lin, H. Hao, L. Mei, M. Wu, Metal-free two-dimensional nanomaterial-mediated photothermal tumor therapy, Smart Mater. Med. 1 (2020) 150–167.
[24] Y. Peng, Y. Huang, Y. Zhu, B. Chen, L. Wang, Z. Lai, Z. Zhang, M. Zhao, C. Tan, N. Yang, F. Shao, Y. Han, H. Zhang, Ultrathin two-dimensional covalent organic framework nanosheets: preparation and application in highly sensitive and selective DNA detection, J. Am. Chem. Soc. 139 (2017) 8698–8704.
[25] X. Liu, D. Huang, C. Lai, G. Zeng, L. Qin, H. Wang, H. Yi, B. Li, S. Liu, M. Zhang, R. Deng, Y. Fu, L. Li, W. Xue, S. Chen, Recent advances in covalent organic frameworks (COFs) as a smart sensing material, Chem. Soc. Rev. 48 (2019) 5266–5302.
[26] X. Kong, Q. Liu, C. Zhang, Z. Peng, Q. Chen, Elemental two-dimensional nanosheets beyond graphene, Chem. Soc. Rev. 46 (2017) 2127–2157.
[27] M.K. Masud, J. Na, M. Younus, M.S.A. Hossain, Y. Bando, M.J.A. Shiddiky, Y. Yamauchi, Superparamagnetic nanoarchitectures for disease-specific biomarker detection, Chem. Soc. Rev. 48 (2019) 5717–5751.
[28] Y. Li, C.X. Yang, X.P. Yan, Controllable preparation of core-shell magnetic covalent-organic framework nanospheres for efficient adsorption and removal of bisphenols in aqueous solution, Chem. Commun. 53 (2017) 2511–2514.
[29] H. Yang, Y. Liu, Z. Guo, B. Lei, J. Zhuang, X. Zhang, Z. Liu, C. Hu, Hydrophobic carbon dots with blue dispersed emission and red aggregation-induced emission, Nat. Commun. 10 (2019) 1789.
[30] S. Lu, L. Sui, J. Liu, S. Zhu, A. Chen, M. Jin, B. Yang, Near-infrared photoluminescent polymer-carbon nanodots with two-photon fluorescence, Adv. Mater. 29 (2017).